2016 IEEE/RSJ International Conference on Intelligent Robots and Systems (IROS)
Daejeon Convention Center
October 9-14, 2016, Daejeon, Korea

Batting Flying Objects to the Target in 2D

Matthew Gardner Yan-Bin Jia
Department of Computer Science
Iowa State University
Ames, IA 50011, USA
mattga, jia@iastate.edu

Huan Lin
Research and Development Center
Yi Jia He Technology Co., Ltd.
Nanjing, Jiangsu, China
linhuanmars@gmail.com

***Abstract*— This paper presents a planning algorithm for a 2-DOF robotic arm to bat a flying 2D object to a targeted location. Impact dynamics are combined with trajectory kinematics and manipulator dynamics to compute the evolving set of states (poses and velocities) of the arm able to achieve the task as the object is flying. Planning is conducted under the arm's dynamic and kinematic constraints. At the time of hit, the robot executes an action to minimize its total energy. Simulation and Experiments have been conducted using a Whole Arm Manipulator (WAM) from Barrett Technology, Inc.**

I. Introduction

Impact happens when two or more bodies collide. Its short duration (< 0.1 second) yields a high impulsive force. Kinetic energy is first stored and then released or transferred among the involved bodies. The resulting impulsive force possesses an efficiency edge over a static or dynamic force. On many occasions, we take advantage of impact to accomplish tasks that would otherwise be difficult, if not impossible. Sports, for instance, is an area where impact is used often in actions like serving a topspin in table tennis, batting a baseball, making a pool shot, etc. Instead of avoiding a collision, the robot should try to utilize it to accomplish a manipulation task more efficiently.

In this paper, we consider the task of batting a flying object to a target point in 2D. The object and bat have known geometries, inertia, and coefficient of restitution. The object's position and velocity just before impact is estimated. Impact planning is performed to determine where to strike the object using a two-link robot with a bat fixed to the end, as well as at what time and velocity to strike in order to perform the task.

Relatively little work exists on impact planning, despite some noticeable efforts on impulsive manipulation [7], [14], [3], [5], and [13]. Impact-based modeling was also used to determine the orientation of an object after bring dropped on a surface [10]. Related to batting, the work [2] focused on the swing trajectory and the force/torque required to generate it, applying Newton's kinematic restitution law [8]. A high-speed robot system [11] was designed for batting the baseball using a hybrid trajectory. The work was then extended to control the direction of the post-impact ball motion [12], though not the entire trajectory. Ball-batting was also achieved with reasonable accuracy using a 4-DOF robot and paddle [4], where the ball's trajectory after impact was considered. Although, both of these approaches lack an impact model that extends to arbitrary shapes as well as frictional impact. Additionally, significant work has been done on ping-pong playing robots, most notably recent work for humanoid robots with a 7-DOF arm [15].

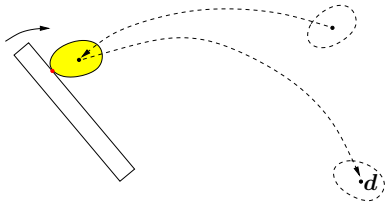

Fig. 1: Batting a flying object to a target at $\boldsymbol{d}$.

We start with a simple version of the batting problem. A self-actuated bat shown in Fig. 1 is controlled to hit a 2D object in order to alter its trajectory to reach a destination point $\boldsymbol{d}$. We assume that there is no contact friction between the bat and the object, which is achievable by choosing their materials to have a high coefficient of friction.

Section II presents impact dynamics and energy-based restitution, and then describes how to obtain the bat's pre-impact motion to drive the object to the destination, when prescribed a hitting configuration. Section III considers a realistic setting of the bat driven by a 2-DOF robotic arm. Combining inverse kinematics, impact dynamics, and motion trajectory, we describe a two-dimensional set of the arm's joint angles and velocities to achieve the batting task. A pre-impact arm state from the set is selected via minimizing the total energy of the arm and the bat. Section IV describes a batting algorithm that plans the arm's motion during the object's flight, and offers some examples. Section V presents results from experiments performed using a robot arm, and the final section discusses immediate and future extensions.

Vectors in the paper are by default column vectors. Since all vectors are planar, the cross product of any two is treated as a scalar (as a coordinate along the orthogonal axis). A tuple is written as a row vector. The subscripts x and y of a letter (not bolded) represent the x- and y-coordinates (or components) of a point (or a vector) named by the same letter (bolded), respectively. For instance, p_x denotes the x-coordinate of the point $\boldsymbol{p}$, while V_{ox} the x-component of a velocity $\boldsymbol{V}_o$. The superscripts '$-$' and '$+$' refer to quantities before and after the impact, respectively. The subscript $\perp$ of a vector $\boldsymbol{v} = (v_x, v_y)^T$ rotates it counterclockwise by $\pi/2$,

that is, $\boldsymbol{v}_\perp = (-v_y, v_x)$ such that $\boldsymbol{v} \times \boldsymbol{u} = \boldsymbol{v}_\perp^T \boldsymbol{u}$ for any vector $\boldsymbol{u}$.

All units are from the metric system. In particular, we use second (s) for time, meter (m) for length, radian (rad) for angle, kilogram (kg) for mass, kilogram square meter ($\mathrm{kg} \cdot \mathrm{m}^2$) for moment of inertia, Newton (N) for force, and Joule (J) for work and energy. Units will be omitted from now on.

II. Two-Dimensional Frictionless Impact

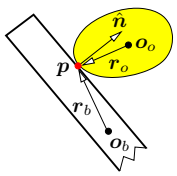

Fig. 2: Impact configuration.

Fig. 2 shows the impact configuration, where the object was flying towards the left just before impact. We assume the position and orientation of the bat and object are known at this moment, as well as the linear and angular velocity of the object. The vectors $\boldsymbol{r}_o$ and $\boldsymbol{r}_b$ locate the contact point $\boldsymbol{p}$ relative to the centers of mass $\boldsymbol{o}_o$ and $\boldsymbol{o}_b$ of the object and the bat, respectively. Without loss of generality, the target $\boldsymbol{d}$ lies to the right of the point of impact $\boldsymbol{p}$. The contact normal $\hat{\boldsymbol{n}} = (n_x, n_y)^T$ has $n_x > 0$, which is a necessary condition for successful batting.

Let m_b be the mass of the bat, and m_o that of the object. Denote by $\boldsymbol{V}_b$ and $\boldsymbol{V}_o$ the velocities of the bat and the object, respectively, and by ω_b and ω_o their angular velocities. The impact changes the object's velocity instantly to $\boldsymbol{V}_o^+ = \boldsymbol{V}_o^- + \Delta\boldsymbol{V}_o$. The object will perform a free flying motion under gravity. Our task here is to plan the bat's pre-impact velocities $\boldsymbol{V}_b^-$ and ω_b^- so the object's trajectory is altered to pass through the destination $\boldsymbol{d}$.

A. Impact Dynamics

Let $\boldsymbol{I}$ be the impulse exerted by the bat on the object. An opposite impulse $-\boldsymbol{I}$ is exerted on the bat by the object under Newton's third law. By Newton's second law, the velocity changes during the impact are

$$\begin{aligned} \Delta\boldsymbol{V}_b &= -\frac{1}{m_b}\boldsymbol{I}, \qquad & \Delta\omega_b &= -\frac{1}{\sigma_b}\boldsymbol{r}_b \times \boldsymbol{I}, \\ \Delta\boldsymbol{V}_o &= \frac{1}{m_o}\boldsymbol{I}, & \Delta\omega_o &= \frac{1}{\sigma_o}\boldsymbol{r}_o \times \boldsymbol{I}, \end{aligned} \tag{1}$$

where σ_b and σ_o are the moments of inertia of the bat and object, respectively. Let $\boldsymbol{v}_b$ and $\boldsymbol{v}_o$ be the velocities of the two points on the bat and the object coinciding at the contact $\boldsymbol{p}$. We have

$$\boldsymbol{v}_b = \boldsymbol{V}_b + \omega_b \boldsymbol{r}_{b\perp} \quad \text{and} \quad \boldsymbol{v}_o = \boldsymbol{V}_o + \omega_o \boldsymbol{r}_{o\perp}. \tag{2}$$

Here, $\boldsymbol{v}_b$ is referred to as the *batting velocity*. The contact velocity is

$$\boldsymbol{v} = \boldsymbol{v}_o - \boldsymbol{v}_b = \boldsymbol{V}_o + \omega_o \boldsymbol{r}_{o\perp} - \boldsymbol{V}_b - \omega_b \boldsymbol{r}_{b\perp}.$$

After plugging in (1), it changes by the amount

$$\begin{aligned} \Delta\boldsymbol{v} &= \Delta\boldsymbol{v}_o - \Delta\boldsymbol{v}_b \\ &= \frac{1}{m_o}\boldsymbol{I} + \frac{\boldsymbol{r}_o \times \boldsymbol{I}}{\sigma_o}\boldsymbol{r}_{o\perp} + \frac{1}{m_b}\boldsymbol{I} + \frac{\boldsymbol{r}_b \times \boldsymbol{I}}{\sigma_b}\boldsymbol{r}_{b\perp} \\ &= W\boldsymbol{I}, \end{aligned} \tag{3}$$

where

$$W = \frac{m_o + m_b}{m_o m_b}\begin{pmatrix} 1 & 0 \\ 0 & 1 \end{pmatrix} + \frac{1}{\sigma_o}\boldsymbol{r}_{o\perp}\boldsymbol{r}_{o\perp}^T + \frac{1}{\sigma_b}\boldsymbol{r}_{b\perp}\boldsymbol{r}_{b\perp}^T \tag{4}$$

is positive definite.

B. Energy-based Restitution

Impact is divided into two phases [9, p. 212]: compression and restitution. During compression, the kinetic energy is transformed into the potential energy E stored at the contact. The phase ends with zero velocity and maximum energy $E_{\max}$. The elastic portion of the stored energy, of the amount $e^2 E_{\max}$, is released during the following restitution phase. Here $e \in [0, 1]$ is referred to as the *energetic coefficient of restitution*. The energy loss by the factor of $1 - e^2$ is due to deformation, heat, etc.

Absence of friction means that there is no impulse or energy exchange along the tangent direction. Hence $\boldsymbol{I} = I\hat{\boldsymbol{n}}$, where I is the impulse magnitude. It is convenient to describe the impact process in terms of I instead of time. The energy function E is differentiable during each impact phase:

$$\frac{dE}{dI} = -\hat{\boldsymbol{n}}^T(\boldsymbol{v}^- + \Delta\boldsymbol{v}) = -v_n^- - \hat{\boldsymbol{n}}^T W \hat{\boldsymbol{n}} I, \tag{5}$$

where $\boldsymbol{v}^-$ is the pre-impact contact velocity, and $v_n^- = \hat{\boldsymbol{n}}^T \boldsymbol{v}^-$ its normal component.

At the end of compression, $dE/dI = 0$, which, after substitution of (5), yields the impulse value $I_c = -v_n^-/(\hat{\boldsymbol{n}}^T S \hat{\boldsymbol{n}})$. Integrate (5) from 0 to I_c to obtain the energy at I_c:

$$E_{\max} = \frac{(v_n^-)^2}{2\hat{\boldsymbol{n}}^T W \hat{\boldsymbol{n}}}. \tag{6}$$

Restitution begins with the energy $e^2 E_{\max}$ and decreases it to zero when the phase ends with the impulse value I_r. We have

$$-e^2 E_{\max} = \int_{I_c}^{I_r} dE, \tag{7}$$

from which we solve for the total impulse:

$$I_r = -\frac{(1+e)(\hat{\boldsymbol{n}}^T \boldsymbol{v}^-)}{\hat{\boldsymbol{n}}^T W \hat{\boldsymbol{n}}} = -\frac{(1+e)v_n^-}{\hat{\boldsymbol{n}}^T W \hat{\boldsymbol{n}}}. \tag{8}$$

C. Bat Motion

With the impact outcome derived, we are now ready to plan the motion of the bat. Substitute (8) into (1):

$$\begin{aligned} \Delta\boldsymbol{V}_o &= \frac{I_r}{m_o}\hat{\boldsymbol{n}} = -\frac{(1+e)v_n^-}{m_o \hat{\boldsymbol{n}}^T W \hat{\boldsymbol{n}}}\,\hat{\boldsymbol{n}} \\ &= -\frac{(1+e)(v_{on}^- - v_{bn}^-)}{m_o \hat{\boldsymbol{n}}^T W \hat{\boldsymbol{n}}}\,\hat{\boldsymbol{n}}, \end{aligned} \tag{9}$$

where $v_{on}^- = \hat{\boldsymbol{n}}^T \boldsymbol{v}_o^-$ and $v_{bn}^- = \hat{\boldsymbol{n}}^T \boldsymbol{v}_b^-$ are the pre-impact normal components of $\boldsymbol{v}_o$ and $\boldsymbol{v}_b$, respectively. Notice that the tangential component of $\boldsymbol{v}_b$ will not affect the motion of the object in the absence of friction. From (9), the object's post-impact velocity is linear in v_{bn}^-:

$$\begin{aligned} \boldsymbol{V}_o^+(v_{bn}^-) &= \boldsymbol{V}_o^- + \Delta\boldsymbol{V}_o \\ &= \boldsymbol{V}_o^- - \frac{(1+e)(v_{on}^- - v_{bn}^-)}{m_o \hat{\boldsymbol{n}}^T W \hat{\boldsymbol{n}}}\hat{\boldsymbol{n}}. \end{aligned} \tag{10}$$

Let $\boldsymbol{q} = \boldsymbol{d} - \boldsymbol{p} + \boldsymbol{r}_o$. For the object to pass through $\boldsymbol{d}$, the following kinematic equation needs to be satisfied:

$$\boldsymbol{q} = \boldsymbol{V}_o^+ t - (0, 0.5g)^T t^2, \tag{11}$$

for some flight time t, where g is the gravitational acceleration. Next, we eliminate t by solving the above system of two equations from the x- and y-coordinates of $\boldsymbol{V}_o^+$ and $\boldsymbol{q}$. This yields an equation in terms of $\boldsymbol{q}$, $\boldsymbol{V}_o^+$, and $\boldsymbol{r}_o$,

$$q_y V_{ox}^{+2} - V_{ox}^+ V_{oy}^+ q_x + 0.5 g q_x^2 = 0. \tag{12}$$

Knowing $\boldsymbol{q}$, we substitute (10) into (12) to obtain a quadratic equation in the normal batting velocity v_{bn}^-. Such a velocity exists if and only if the following two conditions are satisfied:

$$\begin{aligned} \left(n_x \boldsymbol{V}_o^- \times \boldsymbol{q} + V_{ox}^- \hat{\boldsymbol{n}} \times \boldsymbol{q}\right)^2 & \\ - 4 n_x (\boldsymbol{q} \times \hat{\boldsymbol{n}}) \left(0.5 g q_x^2 + V_{ox}^- \boldsymbol{V}_o^- \times \boldsymbol{q}\right) &\geq 0, \quad (13) \\ v_{bn}^- - v_{on}^- &> 0. \quad (14) \end{aligned}$$

The first condition, independent of the masses m_o and m_b, and the restitution coefficient e, ensures that a real root of (12) exists. The second condition, on the root found under the first condition, ensures batting in the positive direction of the normal. Together they are called *task conditions*. The task conditions guarantee the object to reach the destination $\boldsymbol{d}$.

Suppose v_{bn}^- exists. Then by (2), $\hat{\boldsymbol{n}}^T (\boldsymbol{V}_b^- + \omega_b^- \boldsymbol{r}_{b\perp}) = v_{bn}^-$, which implies that all the bat velocities $(\boldsymbol{V}_b, \omega_b)$ to generate v_{bn}^- constitute a plane in the velocity space. The set will be reduced under kinematic and dynamic constraints when a manipulator is used to move the bat, as will be discussed in Section III.

A detailed analysis (omitted for lack of space) has been performed to characterize the region of $(q_x, q_y)^T$ that admits a solution to equation (12). The region is rather large, which means that the bat is capable of sending the object to a wide range of locations.

III. Impact Planning

In a real situation, the bat is attached to a robotic manipulator. This section plans the motion of a two-link arm to carry out the batting task during the flight of an object. We will first work out the arm's inverse kinematics to attain a specific batting configuration. Then we will describe a two-dimensional set of joint angles and velocities with which batting can send an object, at a fixed moment during its flight, to the target. Next, optimization will be introduced to minimize the total energy of the arm and the bat (which measures the work done by the arm). Fig. 3 outlines this procedure along with the vision system used in experiments.

A. Inverse Kinematics

As shown in Fig. 4, we first determine the pose of a two-link robot arm enabling the bat to hit the flying object at $\boldsymbol{p}$. Suppose that the contact normal $\hat{\boldsymbol{n}}$ is known. The two links attached to the arm joints J_1 and J_2 have lengths l_1 and l_2,

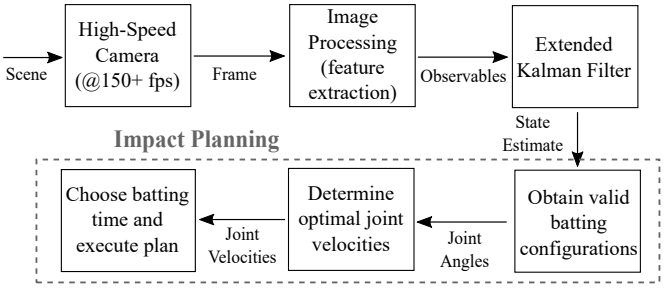

Fig. 3: Block diagram of impact planning and computer vision.

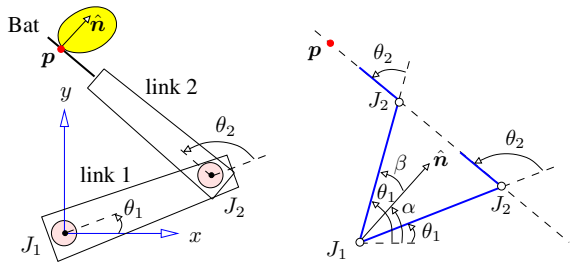

Fig. 4: Inverse kinematics: (a) actual configuration and (b) two possible configurations (θ_1, θ_2) in which the second link has the normal $\hat{\boldsymbol{n}}$ and is incident on $\boldsymbol{p}$.

respectively. Let l_b be the length of the bat. We would like to determine the joint angles θ_1 and θ_2.

The origin is placed at J_1. The unit vectors along the two links are

$$\hat{\boldsymbol{l}}_1 = \begin{pmatrix} \cos\theta_1 \\ \sin\theta_1 \end{pmatrix} \quad \text{and} \quad \hat{\boldsymbol{l}}_2 = \begin{pmatrix} \cos(\theta_1 + \theta_2) \\ \sin(\theta_1 + \theta_2) \end{pmatrix}. \tag{15}$$

Thus, J_2 is at the location $l_1 \hat{\boldsymbol{l}}_1$, and we set up three conditions:

$$\begin{aligned} \hat{\boldsymbol{n}}^T \hat{\boldsymbol{l}}_2 &= 0, & (16) \\ \hat{\boldsymbol{n}}^T (\boldsymbol{p} - l_1 \hat{\boldsymbol{l}}_1) &= 0, & (17) \\ \hat{\boldsymbol{l}}_2^T (\boldsymbol{p} - l_1 \hat{\boldsymbol{l}}_1) &\in (l_2, l_2 + l_b]. & (18) \end{aligned}$$

Equation (17) implies that $|\hat{\boldsymbol{n}}^T \boldsymbol{p}/l_1| = |\hat{\boldsymbol{n}}^T \hat{\boldsymbol{l}}_1| \leq 1$. Thus, batting at $\boldsymbol{p}$ can be performed only if the *reachability condition* below is satisfied:

$$-l_1 \leq \hat{\boldsymbol{n}}^T \boldsymbol{p} \leq l_1. \tag{19}$$

Let α be the polar angle of $\hat{\boldsymbol{n}}$, and $\beta = \cos^{-1}(\hat{\boldsymbol{n}}^T \boldsymbol{p}/l_1)$. See Fig. 4(b). Then we have

$$\theta_1 = \alpha \pm \beta, \tag{20}$$

corresponding to two possible configurations of link 1.

Substitute (15) for $\hat{\boldsymbol{l}}_2$ into (16) and rewrite it as

$$\cos\theta_2 \left(\hat{\boldsymbol{l}}_1^T \hat{\boldsymbol{n}}\right) + \sin\theta_2 (\hat{\boldsymbol{l}}_1 \times \hat{\boldsymbol{n}}) = 0.$$

Since the vector $(\hat{\boldsymbol{l}}_1^T \hat{\boldsymbol{n}}, \hat{\boldsymbol{l}}_1 \times \hat{\boldsymbol{n}})^T$ is unit, the above yields $(\cos\theta_2, \sin\theta_2) = \pm(\hat{\boldsymbol{n}} \times \hat{\boldsymbol{l}}_1, \hat{\boldsymbol{n}}^T \hat{\boldsymbol{l}}_1)$, from which we obtain

$$\theta_2 = \pi \pm \operatorname{atan2}(\hat{\boldsymbol{n}}^T \hat{\boldsymbol{l}}_1, \hat{\boldsymbol{n}} \times \hat{\boldsymbol{l}}_1). \tag{21}$$

In the above, the sign is uniquely chosen under condition (18) because $\hat{\boldsymbol{l}}_2$ must be in the direction of $\boldsymbol{p} - J_2$. Thus, for each θ_1 value, at most one θ_2 value exists. In summary, conditions (16)–(18) induce at most two possible values of (θ_1, θ_2), for which the configurations are drawn in Fig. 4(b).

B. Configuration Space of Contact

For simplicity we assume convexity of the object. At the time of impact, its center of mass $\boldsymbol{o}_o$ is at $\boldsymbol{p} - \boldsymbol{r}_o$ (cf. Fig. 2), where its body frame has a rotation from the world frame described by the matrix R. Let the curve $\boldsymbol{\gamma}(s) = (\gamma_x(s), \gamma_y(s))^T$ describe the object's boundary in the body frame such that the parameter s increases counterclockwise. By a slight abuse of notation, we let s locate the contact point $\boldsymbol{p}$ on $\boldsymbol{\gamma}$, i.e., $R\boldsymbol{\gamma}(s) = \boldsymbol{r}_o$. The contact normal is thus

$$\hat{\boldsymbol{n}}(s) = R(-\gamma_y', \gamma_x')^T / \|\boldsymbol{\gamma}'\|. \tag{22}$$

Below we describe the set of (θ_1, θ_2) values that satisfy the constraints (16)–(18) as the contact point

$$\boldsymbol{p}(s) = \boldsymbol{o}_o + R\boldsymbol{\gamma}(s) \tag{23}$$

varies along the object's boundary under the conditions (19) and $n_x > 0$.

Since $\hat{\boldsymbol{n}}$ and $\boldsymbol{p}$ depend on s, so do the angles α and β. Equation (20) defines θ_1 as a function of s, where the sign '$+$' or '$-$' is chosen over different intervals of θ_1. In the joint angle space, as s varies, all (θ_1, θ_2) that result in the bat making contact with the object form curve segments on the object's boundary. These segments are further reduced by the joint ranges Θ_1 of θ_1 and Θ_2 of θ_2.

C. Configurations for Batting

Consider an arm pose $(\theta_1, \theta_2(\theta_1))$ allowing the bat to be in contact with the object at the current time instant. For convenience, the contact point on the bat is $l_1\hat{\boldsymbol{l}}_1 + a\hat{\boldsymbol{l}}_2$, where $a = \hat{\boldsymbol{l}}_2^T(\boldsymbol{p} - l_1\hat{\boldsymbol{l}}_1)$ depends on θ_1 and θ_2. The velocity of the contact point just before the impact is obtained through differentiation while treating a as a constant:

$$\boldsymbol{v}_b^- = \left(l_1\hat{\boldsymbol{l}}_{1\perp} + a\hat{\boldsymbol{l}}_{2\perp}\right)\dot{\theta}_1 + a\hat{\boldsymbol{l}}_{2\perp}\dot{\theta}_2. \tag{24}$$

For $k = 1, 2$ let m_k be the mass of link k, σ_k its moment of inertia about the joint J_k, and d_k the distance from its center of mass to the joint J_k. Let d_b be the distance from the bat's center of mass to the joint J_2. Then the bat's moment of inertia about J_1 is $\bar{\sigma}_b = \sigma_b + m_b\|l_1\hat{\boldsymbol{l}}_1 + d_b\hat{\boldsymbol{l}}_2\|^2$.

At the moment of impact, we consider the arm to be rigidly connected with the bat, which exerts an impulsive force on the flying object, as well as links 1 and 2 of the arm [1, p. 18]. From dynamics, we have

$$\Delta\dot{\theta}_1 = -\frac{l_1}{\sigma_1}\hat{\boldsymbol{l}}_1 \times \boldsymbol{I} \quad \text{and} \quad \Delta\dot{\theta}_2 = -\frac{a}{\bar{\sigma}_2 + \bar{\sigma}_b}\hat{\boldsymbol{l}}_2 \times \boldsymbol{I},$$

where the inertia of link 2 about J_1 is $\bar{\sigma}_2 = \sigma_2 + m_2 l_1^2$.

The velocity $\boldsymbol{v}_o$ of the contact point on the object is still given in (2). The change in the contact velocity $\Delta\boldsymbol{v}$ assumes the same form as (3), except from (24) we now have

$$W = \frac{1}{m_o}\begin{pmatrix}1 & 0\\ 0 & 1\end{pmatrix} + \frac{1}{\sigma_o}\boldsymbol{r}_{o\perp}\boldsymbol{r}_{o\perp}^T + \frac{l_1}{\sigma_1}\hat{\boldsymbol{l}}_{1\perp}\left(l_1\hat{\boldsymbol{l}}_{1\perp}^T + a\hat{\boldsymbol{l}}_{2\perp}^T\right) + \frac{a^2}{\bar{\sigma}_2 + \bar{\sigma}_b}\hat{\boldsymbol{l}}_{2\perp}\hat{\boldsymbol{l}}_{2\perp}^T.$$

For the pre-impact normal velocity $v_{bn}^- = \hat{\boldsymbol{n}}^T\boldsymbol{v}_b^-$ to exist, the task conditions (13) and (14) must be satisfied by the normal $\hat{\boldsymbol{n}}$ and $\boldsymbol{q} = \boldsymbol{d} - \boldsymbol{p} + \boldsymbol{r}_o$. After substitutions of (22) and (23), the conditions are on the parameter s locating the contact point. Meanwhile, every (θ_1, θ_2) satisfying conditions (16)–(18) and lying in the joint angle ranges determines an s value. Namely, s is a function of θ_1. The task conditions are thus imposed on θ_1, though their forms in terms of θ_1 cannot be written out compactly[1].

The task conditions (13) and (14) further reduce those (θ_1, θ_2) segments from Section III-B, which already ensures the bat's contact with the object and that the joint ranges Θ_1 and Θ_2 are not exceeded. Every pair (θ_1, θ_2) on a resulting segment is called a *feasible pose*.

The arm will be based on a 4-DOF WAM arm, where θ_1 and θ_2 refer to the angles of its joints 2 and 4, and the other two joints are not used. Table I gives the values of physical parameters related to the two links, the bat, and the object.

$l_1 = 0.55$,	$d_1 = 0.3426$,	$m_1 = 5.6772$,	$\sigma_1 = 0.2929$,
$l_2 = 0.35$,	$d_2 = 0.1446$,	$m_2 = 1.0651$,	$\sigma_2 = 0.0412$,
$l_b = 0.265$,	$d_b = 0.4423$,	$m_b = 0.3433$,	$\sigma_b = 0.0704$,
		$m_o = 0.0175$,	$\sigma_o = 0.0000355$,
$\Theta_1 = [-0.429, 3.571]$,		$\Omega_1 = [-0.85, 0.85]$,	$\Phi_1 = [-8, 8]$,
$\Theta_2 = [\mp 0.9, \pm 3.1]$,		$\Omega_2 = [-5, 5]$,	$\Phi_2 = [-60, 60]$.

TABLE I: Values of physical parameters. The first four rows display the lengths, masses, and moments of inertia of the two links, the bat, and the elliptic object in Figs. 5. The last two rows display the ranges Θ_i, Ω_i, and Φ_i, $i = 1, 2$, of joint i's angle, velocity, and acceleration. Joint angle ranges are relative to the zero position. The range Θ_2 is either $[-0.9, 3.1]$ or $[-3.1, 0.9]$ by controlling the WAM's third joint.

Consider an example where a solid, elliptic object[2] is thrown from the location $(1.5, 0.7)$, with velocity $(-2.8, 1.2)$, and rotating at a constant rate of 10. Fig. 5 plots the evolution of feasible arm poses (θ_1, θ_2) over 0.53 seconds of flight. At time 0.29, the feasible poses form the red curve in the plot, and the red segment of contact points on the corresponding ellipse. The cross on the red curve at $(0.559, 0.621)$ produces the batting configuration drawn out.

At time 0.45, the object is within reach of two feasible poses that form the green curve segments marked by c_2 and c_3. The curve segment c_1 includes poses where only a smaller θ_1 value can reach the object, while the curve segment c_4

[1] In computation it is easier to first find the s values, each corresponding to up to two θ_1 values.

[2] The object has its semi-major and semi-minor axes of length 0.075 and 0.05 aligned, under no rotation, with the x- and y-axes, respectively. Its physical parameters are shown in Table I.

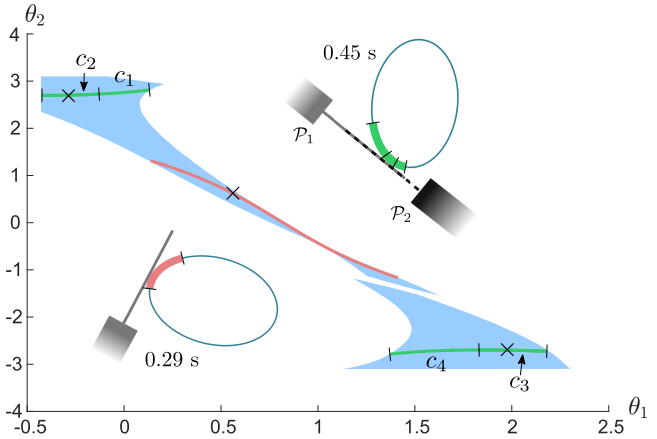

Fig. 5: (a) Regions of the arm poses for batting an object bounded by an ellipse. Batting configurations are superimposed for time 0.29 when the object is located at $(0.688, 0.636)^T$ with a rotation of 2.9, and at time 0.45 when at $(0.433, 0.881)$ with a rotation of 4.5.

includes those with a larger θ_1. The resulting segment of contact points are drawn on the corresponding ellipse along with two batting configurations that reach the same contact point. The cross on c_2 at $(-0.178, 2.62)$ produces the arm pose $\mathcal{P}_2$, while the cross on c_3 at $(1.921, -2.62)$ produces the pose $\mathcal{P}_1$.

D. Feasible Arm Motions

We now consider how to find the joint velocities $\dot{\theta}_1$ and $\dot{\theta}_2$ for batting. Given a feasible pose $(\theta_1, \theta_2(\theta_1))$, the pre-impact normal velocity v_{bn}^- exists to complete the batting task. It is solved from the quadratic equation resulting from a substitution of (10) into (12). Up to two roots exist. It follows from equation (24) that

$$v_{bn}^- = -(l_1 \cos\theta_2 + a)\dot{\theta}_1 - a\dot{\theta}_2$$

where we make use of $\hat{\boldsymbol{n}} = -\hat{\boldsymbol{l}}_{2\perp}$ and $\hat{\boldsymbol{n}}^T\hat{\boldsymbol{l}}_{1\perp} = -\hat{\boldsymbol{l}}_2^T\hat{\boldsymbol{l}}_{1\perp} = -\cos\theta_2$. Since $\hat{\boldsymbol{n}}$, $\hat{\boldsymbol{l}}_{1\perp}$, and $\hat{\boldsymbol{l}}_{2\perp}$ all depend on θ_1, the above equation defines $\dot{\theta}_2$ as a function of θ_1 and $\dot{\theta}_1$:

$$\dot{\theta}_2(\theta_1, \dot{\theta}_1) = -v_{bn}^- - (l_1 \cos\theta_2 + a)\,\dot{\theta}_1. \tag{25}$$

Thus, the two variables θ_1 and $\dot{\theta}_1$ completely characterize the arm's *state* (configuration and velocity).

Next, we determine the range of $\dot{\theta}_1$ given θ_1. Suppose that the robot starts moving at time τ ahead of when the object reaches the impact configuration. We let every joint k, $k = 1, 2$, accelerate at a constant rate for some initial time period τ_k to reach $\dot{\theta}_k$, and then maintain the velocity for the remaining period $\tau - \tau_k$ until the joint angle reaches θ_k. Under this acceleration scheme, the following two conditions hold:

$$\dot{\theta}_k \cdot \theta_k > 0, \qquad k = 1, 2. \tag{26}$$

Both conditions above are imposed on θ_1 and $\dot{\theta}_1$. It is easy to derive that

$$\dot{\theta}_k \left(\tau - \frac{\tau_k}{2}\right) = \theta_k, \qquad k = 1, 2, \tag{27}$$

which, under (26) and (27), ensure only $\tau > \tau_1/2, \tau_2/2$. So, we must also enforce the constraints $\tau > \tau_1, \tau_2$. Subtracting the two equations in (27) and combining it with $\tau > \tau_2$ yields a second constraint on τ_1:

$$\tau > \tau_1 + 2\left(\frac{\theta_1}{\dot{\theta}_1} - \frac{\theta_2}{\dot{\theta}_2}\right). \tag{28}$$

The arm must also be able to accelerate to $\dot{\theta}_1$ and $\dot{\theta}_2$ within τ_1 and τ_2, respectively. Let $\delta_1, \delta_2 > 0$ be the maximum accelerations[3] for joints 1 and 2. Then, the following conditions must be satisfied:

$$\tau_k \delta_k \geq |\dot{\theta}_k|, \qquad k = 1, 2. \tag{29}$$

Additionally, enough time must be provided for planning and transmission of data over the network (to the WAM arm):

$$\tau \leq \tau_{\max} - \tau_p \tag{30}$$

where $\tau_{\max}$ is the period between the time that planning starts and the time of impact, and τ_p is the worst-case time for planning and data transmission to finish.

Equation (27) allows us to convert any constraint involving τ_2 into one involving τ_1 (as done with inequality (28)). We then obtain the upper and lower bounds of τ_1 that satisfy constraints (26) and (28)-(30) when the following holds:

$$\begin{aligned} &\max\left\{\frac{|\dot{\theta}_1|}{\delta_1},\ \frac{|\dot{\theta}_2|}{\delta_2} - 2\left(\frac{\Delta\theta_1}{\dot{\theta}_1} - \frac{\Delta\theta_2}{\dot{\theta}_2}\right)\right\} \\ &\leq \min\left\{\frac{2\Delta\theta_1}{\dot{\theta}_1},\ \frac{4\Delta\theta_2}{\dot{\theta}_2} - \frac{2\Delta\theta_1}{\dot{\theta}_1},\ 2\left(\tau_{\max} - \tau_p - \frac{\Delta\theta_1}{\dot{\theta}_1}\right)\right\} \end{aligned} \tag{31}$$

Once the inequality holds, there exists one value of τ_1 between its left and right hand sides, and one value each of τ_2 and τ as determined from (27). The original constraints (26) and (28)–(30) can be easily realized from (31) (proof omitted for space).

Furthermore, this interval defines the space of $(\theta_1, \dot{\theta}_1)$ solutions that can successfully accomplish the batting task. Given θ_1 (and thus θ_2), constraints (26) and (31) when combined with (25) break down into eight inequalities[4]. These are applied together with the range Ω_i for $\dot{\theta}_i$, $i = 1, 2$, to obtain an interval $[\eta_a(\theta_1), \eta_b(\theta_1)]$. After choosing $\dot{\theta}_1$ from this interval (see Section III-E), θ_2 and $\dot{\theta}_2$ are calculated from (21) and (25), and τ_1 is chosen to be the average of the left and right hand sides of (31). The choice of τ_1 is for robustness to control uncertainties and measurement error, which the solution is more vulnerable to towards the boundaries.

E. Batting with Minimum Effort

Our next step is to minimize the batting effort, which is characterized as the total mechanical energy of the bat and the two-link arm. This ensures that both arm joints exert minimal work in order to achieve the batting task. The kinetic

[3]Namely, the acceleration range is $\Phi_i = [-\delta_i, \delta_i]$, $i = 1, 2$.

[4]two of the inequalities are linear, four are quadratic, and three are cubic

energies of the two links and the bat can be derived as follows:

$$T_1 = \frac{1}{2}\sigma_1\dot{\theta}_1^2,$$
$$T_i = \frac{1}{2}\sigma_i\dot{\theta}_2^2 + \frac{1}{2}m_i l_1^2\dot{\theta}_1^2 + m_i d_i l_1 \cos\theta_2 \left(\dot{\theta}_1^2 + \dot{\theta}_1\dot{\theta}_2\right),$$

for $i = 2, b$. Meanwhile, their potential energies are

$$U_1 = m_1 g d_1 \sin\theta_1,$$
$$U_i = m_i g\Big(l_1 \sin\theta_1 + d_i \sin(\theta_1 + \theta_2)\Big), \quad i = 2, b.$$

The total energy of the arm is thus

$$E(\theta_1, \dot{\theta}_1) = T_1 + T_2 + T_b + U_1 + U_2 + U_b.$$

Minimization of E is carried out in two steps: first over $\dot{\theta}_1$ given θ_1, and then over all discretized θ_1 values. We first discretize the subdomain of the object's boundary curve $\boldsymbol{\gamma}(s)$ with inward normal $\boldsymbol{n}$ satisfying $n_x > 0$. Let $s_1, s_2, \ldots, s_n$ be the discretized values that also satisfy the reachability (19), and the task conditions (13) and (14). For every s_k, we substitute in (23) for $\boldsymbol{p}$, and solve for up to two $(\theta_1(s_k), \theta_2(s_k))$ values that satisfy conditions (16)–(18) and fall within the arm's joint angle range. For each feasible $(\theta_1(s_k), \theta_2(s_k))$, use the method in Section III-D to obtain the interval $[\eta_a(\theta_1), \eta_b(\theta_1)]$ of feasible joint velocity values $\dot{\theta}_1$.

For simplicity, rewrite (25) as $\dot{\theta}_2 = \lambda_1 + \lambda_2\dot{\theta}_1$ where

$$\lambda_1(\theta_1) = \frac{v_{bn}^-}{a\hat{\boldsymbol{n}}^T\hat{\boldsymbol{l}}_{2\perp}} \quad \text{and} \quad \lambda_2(\theta_1) = -1 - \frac{l_1\hat{\boldsymbol{n}}^T\hat{\boldsymbol{l}}_{1\perp}}{a\hat{\boldsymbol{n}}^T\hat{\boldsymbol{l}}_{2\perp}}.$$

With θ_1 and θ_2 treated as constants and $\dot{\theta}_2$ as a function, the derivative $dE/d\dot{\theta}_1$ vanishes at

$$\eta_c(\theta_1) = -\Big((\sigma_2 + \bar{\sigma}_b)\lambda_1\lambda_2 + (m_2 d_2 + m_b d_b) l_1 \lambda_1 \cos\theta_2\Big) \Big/ \Big(\sigma_1 + (\sigma_2 + \bar{\sigma}_b)\lambda_2^2 + (m_2 + m_b) l_1^2 + 2(m_2 d_2 + m_b d_b) l_1 \cos\theta_2 (1 + \lambda_2)\Big).$$

Then the minimum of E over $[\eta_a(\theta_1), \eta_b(\theta_1)]$ for a given θ_1 must be achieved at either of the two endpoints, or at $\eta_c(\theta_1)$ if $\eta_c(\theta_1) \in [\eta_a(\theta_1), \eta_b(\theta_1)]$. Denote by $\xi(\theta_1)$ the value of $\dot{\theta}_1$ at which the minimum is achieved.

We then minimize E over all $(\theta_1, \xi(\theta_1))$ that have a feasible pose $(\theta_1, \theta_2(\theta_1))$ (from Section III-A) and non-empty interval $[\eta_a(\theta_1), \eta_b(\theta_1)]$ (from Section III-D). Thus, the resulting optimal pose and motion is $(\theta_1^*, \xi(\theta_1^*))$.

IV. Batting Algorithm and Simulation

Algorithm 1 combines the components from Section III to control the arm to execute a batting operation. The algorithm assumes a Kalman filter (KF) to constantly estimate the motion of the flying object. Planning starts immediately when the estimate of the object's motion converges enough (line 3). At this moment, it hypothesizes the hit to happen at time $t + \tau_{\max}$ (line 5) and checks for feasible states of the arm (lines 6–8). If the set of feasible states is big enough, it computes the optimal arm movement and executes the batting operation (lines 10-16). In the case that no good set of feasible states are found, it looks for a later hitting time, and repeats so until the object is out of reach (lines 5–19). The outer while loop of lines 3–22 iterates at the next time instant of the object's flight.

Algorithm 1 Batting a flying object

1: **while** the object is flying at time t **do**
2: a Kalman filter continues to estimate its motion
3: **if** the motion estimate converges enough **then**
4: calculate the time t_e when the object is beyond reach
5: **while** $\tau_{\max} \le t_e - t$ **do**
6: predict the object's state at $t + \tau_{\max}$
7: discretize boundary points satisfying (19), (13), (14) at time $t + \tau_{\max}$
8: compute $P = \{\theta_1 \mid (\theta_1, \theta_2(\theta_1))$ feasible$\}$
9: **if** P is reasonably large **then**
10: compute $[\eta_a(\theta_1), \eta_b(\theta_1)]$, $\eta_c(\theta_1)$ for all $\theta_1 \in P$
11: determine the optimal arm state $(\theta_1^*, \xi(\theta_1^*))$
12: $\tau_1 \leftarrow$ average of LHS and RHS in (31)
13: set τ and τ_2 according to (27)
14: $\ddot{\theta}_k \leftarrow \frac{\Delta\theta_k^*}{\tau_k^2}$, $k = 1, 2$
15: start moving link i at time $t + \tau_{\max} - \tau$, $i = 1, 2$
16: **return** success
17: **end if**
18: increment $\tau_{\max}$
19: **end while**
20: **end if**
21: adjust clock time t
22: **end while**
23: **return** failure

Consider the same scenario of the elliptic object from Fig. 5. Impact happens at time 0.39 when the object is at the position $(0.408, 0.423)^T$, with a rotation of 3.9. Fig. 6(a) plots the region of feasible states for the WAM Arm at this moment. The gray, blue, and orange curves, which extend out along the dashed gray lines, are the constraints from (31) that bound the solution space (in green). The constraints are labeled by their corresponding inequalities (on the sides where the feasible regions lie). The remaining constraints are easily satisfied with the equality curves lying outside the displayed region. The black curve cutting through the solution space is the curve of arm states at which the partial derivative of E over $\dot{\theta}_1$ diminishes, that is, $\eta_c(\theta_1) \in [\eta_a(\theta_1), \eta_b(\theta_2)]$. For θ_1 values to the left and right of the curve $\eta_c(\theta_1)$, the minimal energy solutions continue along the orange and blue constraints, respectively.

The range of θ_1 of feasible poses has been reduced from $(-0.429, 2.301)$ (see Fig. 5), to $(-0.286, -0.154)$ after removing those values that yield no feasible $\dot{\theta}_1$. The optimal state (green point) and a non-optimal state (red point) are selected for comparison from the feasible region in (a). The optimal state expands to $\boldsymbol{x} = (\theta_1, \theta_2, \dot{\theta}_1, \dot{\theta}_2) = (-0.286, 2.182, -0.85, -2.868)$ with

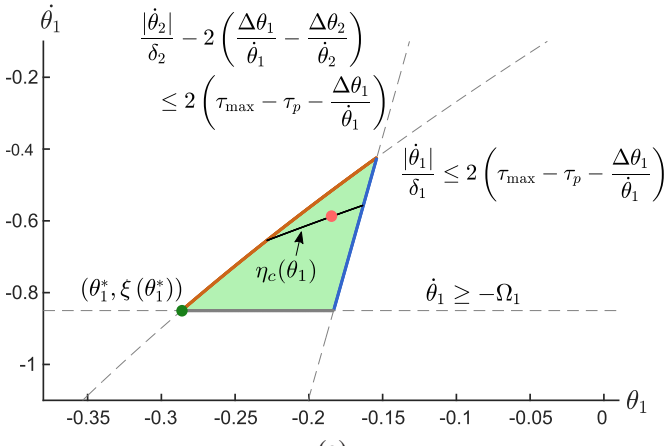

(a)

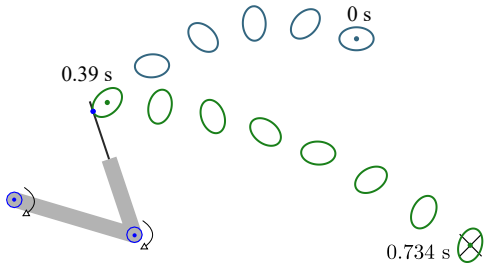

(b)

Fig. 6: (a) Region of feasible $(\theta_1, \dot{\theta}_1)$. A non-optimal solution is marked by the red point. The optimal state $(\theta_1^*, \xi(\theta_1^*))$, marked by the green point, is drawn out in (b) where the elliptic object's incoming trajectory is blue, and outgoing trajectory is green. Values of relevant physical parameters are found in Table I.

-3.602 energy, while the sub-optimal state expands to $\boldsymbol{x} = (-0.184, 2.137, -0.588, -2.450)$ with -1.817 energy[5]. Their batting outcomes result in similar outgoing trajectories, of which the optimal trajectory is shown in (b). The coefficient of restitution $e = 0.8$ is used for the batting.

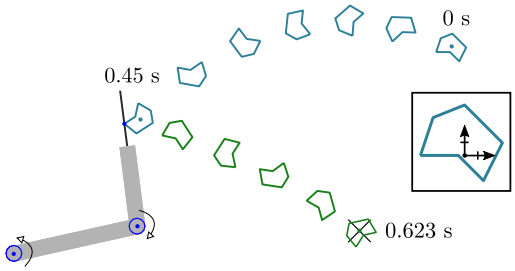

Fig. 7: Batting a polygon to $\boldsymbol{d} = (1.5, .1)^T$. Initial joint angles are $\theta_1 = 0$ and $\theta_2 = 3$. The inset shows the polygon with respect to it's reference frame at the origin and with zero rotation.

Fig. 7 plots the batting of an incoming 6-sided polygon[6] with the same mass 0.0175 as the ellipse, and the moment of inertia .0000267 with respect to the center of mass. At time 0, the polygon is located at $(1.9, 0.9)^T$. Impact happens at time 0.45 when the object reaches $(0.550, 0.582)^T$ with a rotation of 4.5, velocity of $(-3.0, -2.91)^T$, and angular velocity of 10. The contact point $(0.479, 0.564)^T$ and normal $(0.992, 0.127)^T$ are manually chosen to avoid parameterizing the polygon's boundary. The arm's expanded state is $\boldsymbol{x} = (0.219, 1.479, 0.525, -4.884)$. The post-impact velocities are $(5.493, -1.821)^T$ and 52.455, and the object reaches the target at time 0.623.

[5]Negative energy is obtained due to potential energy being relative to the zero value of J_1

[6]Its six vertices about the origin are $(-0.07, 0.0)$, $(-0.05, 0.06)$, $(0.0, 0.08)$, $(0.06, 0.02)$, $(0.03, -0.04)$, and $(-0.01, 0.0)$.

V. Experiment

Experiments were performed with a standard ping-pong ball (mass: 2.7g, radius: 2 cm), and a $2\frac{1}{2}$D cork hexagon of mass 0.086 and inertia 0.0000969. A 4-DOF WAM arm from Barrett Technology was used with an acrylic paddle attached as an end effector. The paddle had a length of 0.265, mass of 0.343, and inertia of 0.0032. The bat had a coefficient of restitution of 0.39 with the hexagon, and 0.777 with the ping-pong ball. Angular velocity and orientation of the ball were ignored. Physical parameters of the WAM arm are listed in Table I.

To provide accurate estimation of the object's motion, a vision system was developed using a Ximea MQ022CG-CM high-speed camera with a Navitar NMV-6 wide-angle lens. Two line segments were marked on the object in the shape of a "T", allowing for its orientation to be uniquely determined through image processing. The choice of line segment features was to provide more data to be fit with a line for a more accurate measurement. Observed values from each frame were then input into an Extended Kalman Filter that models air drag and lens distortion, and outputs an estimate of the object's position, velocity, orientation, and angular velocity. These estimates were then input into the planning algorithm. Through various optimizations, the process of motion estimation, impact planning, and data transmission took less than 5.2 ms, allowing for more than 150 frames to be processed per second.

	Missed Object	Missed Target	Close (< 0.3 m)	Success (< 0.1 m)
Ping-pong Ball	20 (33.3%)	10 (16.7%)	19 (31.7%)	11 (18.3%)
Cork Hexagon	15 (48.4%)	4 (12.9%)	8 (25.8%)	4 (12.9%)

TABLE II: Summary of batting results.

Objects were thrown by hand from more than 3 meters away so that enough data was produced for estimation. Results were evaluated by the object's distance from the target point, where within 0.1 m was considered a success, within 0.4 m was close, and anything further was a miss. Instances where the bat swung, but missed the object, were also recorded. Table II summarizes results from many throws of the ping-pong ball and hexagon, of which 60 and 31 throws, respectively, stayed in the 2D plane and had a solution found.

Other than human error in throwing the object, the primary source of error was in predicting the location and velocities of the object at impact, causing the bat to occasionally

miss the object. Actuation error of the arm was addressed by adjusting gain values of the WAM's PID controller, which determines how effectively the commanded values are obtained. Errors in the robot's joint positions were reduced to within 0.0026 and 0.016 for joints 1 and 2, respectively, and within 0.012 and 0.065 for the joint velocities.

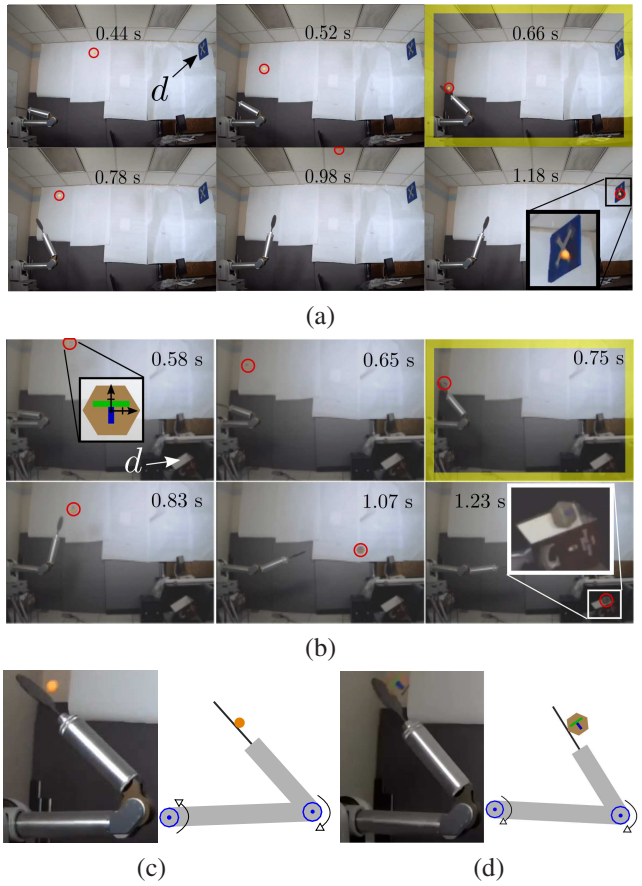

Fig. 8: Two sequences of video frames for batting (a) a ping-pong ball to a hanging target, and (b) a hexagon to a target at the opening of a box. The frames at which impact happens are highlighted yellow. The batting configurations (from both simulation and experiment) for the two scenarios are shown in (c) and (d).

Fig. 8 shows two sequences of images with each object successfully reaching different targets. The ping-pong ball in (a) was batted at the arm state $\boldsymbol{x} = (0.038, 2.262, 0.086, -3.276)$ to the target hanging at $\boldsymbol{d} = (2.553, 1.016)$ (marked by a white cross on a blue sheet). Impact planning finished at time 0.214 after receiving 33 frames of data. The time of impact was predicted to happen $\tau_{\max} = 0.45$ seconds later, and the timings for acceleration were set to $\tau_1 = 0.011$ and $\tau_2 = 0.439$. A closeup of the batting configuration is shown in (c) alongside the drawn out solution.

In (b), a solution with the hexagon was found at time 0.449 when 64 frames had been processed. In the first frame, the object is inset with a rotation of zero. The hexagon was parameterized at vertices that could be batted rightward. At each vertex, 11 discretized contact normals were considered. The object was batted at the arm state $\boldsymbol{x} = (-0.052, 2.163, -0.352, -4.769)$ to the target in the box at $\boldsymbol{d} = (2.286, -0.495)$. The timings were $\tau_{\max} = 0.3$, $\tau_1 = 0.215$ and $\tau_2 = 0.159$.

VI. Ongoing and Future Work

One improvement on Algorithm 1 will be to adjust the planned arm motion as more accurate motion estimates are obtained. Experiments will be improved by a mechanism for repeatable throws, and objects constructed from more ideal materials. We will also extend planning to consider contact friction. The approach remains the same, but the task condition (13) does not have a clean form. A case-by-case analysis of frictional impact is done and efficient numerical methods are used to obtain joint velocities.

Another extension will be to 3D batting. Technical challenges will include estimation of linear and angular motions of the flying object, and sophisticated planning algorithm design. Tangential compliance [6] may not be ignored as they may play a significant role affecting the impact outcome.

VII. Acknowledgment

Support of this research was provided by the National Science Foundation through the grant IIS-1421034. The authors would like to thank Xiaoqian Mu and Jiale Feng for their help with the experiments and vision system. Any opinions, findings and thoughts discussed in this material are those of the authors and do not necessarily reflect the views of the National Science Foundation.

References

[1] Antal K Bejczy. Robot arm dynamics and control. 1974.
[2] R. Cross. Mechanics of swinging a bat. *American Journal of Physics*, 77(1):36–43, 2009.
[3] S. Hirai, M. Niwa, and S. Kawamura. Development of impulsive object sorting device with air floating. In *ICRA*, pages 3065–3070, 1999.
[4] T. Hsiao, C-M. Yang, I-H. Lee, and C-C. Hsiao. Design and implementation of a ball-batting robot with optimal batting decision making ability. In *Int. Conf. Automation Science and Engineering (CASE)*, pages 1026–1031. IEEE, 2014.
[5] W. H. Huang and M. T. Mason. Mechanics, planning, and control for tapping. *Int. J. of Robotics Research*, 19(10):883–894, 2000.
[6] Y-B. Jia, M. T. Mason, and M. Erdmann. Multiple impacts: A state transition diagram approach. *International Journal of Robotics Research*, 32(1):84–114, 2013.
[7] J. B. Keller. Impact with friction. *Journal of applied Mechanics*, 53(1):1–4, 1986.
[8] P. Kirkpatrick. Batting the ball. *American Journal of Physics*, 31(8):606–613, 1963.
[9] M. T. Mason. *Mechanics of robotic manipulation*. MIT press, 2001.
[10] Mark Moll and Michael A Erdmann. Manipulation of pose distributions. *Int. J. of Robotics Research*, 21(3):277–292, 2002.
[11] T. Senoo, A. Namiki, and M. Ishikawa. High-speed batting using a multi-jointed manipulator. In *In Proc. Int. Conf. Robotics and Automation*, volume 2, pages 1191–1196. IEEE, 2004.
[12] T. Senoo, A. Namiki, and M. Ishikawa. Ball control in high-speed batting motion using hybrid trajectory generator. In *In Proc. Int. Conf. on Robotics and Automation*, pages 1762–1767. IEEE, 2006.
[13] K. Tagawa, K. Hirota, and M. Hirose. *Manipulation of dynamically deformable object using impulse-based approach*. INTECH Open Access Publisher, 2010.
[14] Y-T Wang, V. Kumar, and J. Abel. Dynamics of rigid bodies undergoing multiple frictional contacts. In *In Proc. Int. Conf. Robotics and Automation*, pages 2764–2769. IEEE, 1992.
[15] Z. Yu, Y. Liu, Q. Huang, X. Chen, W. Zhang, J. Li, et al. Design of a humanoid ping-pong player robot with redundant joints. In *Int. Conf. Robotics and Biomimetics*, pages 911–916. IEEE, 2013.